11-1-2021

Ultracompact fluorescence smartphone attachment using built-in optics for protoporphyrin-IX quantification in skin

Brady Hunt
Thayer School of Engineering at Dartmouth

Samuel S. Streeter
Thayer School of Engineering at Dartmouth

Alberto J. Ruiz
Thayer School of Engineering at Dartmouth

M. Shane Chapman
Geisel School of Medicine at Dartmouth

Brian W. Pogue
Thayer School of Engineering at Dartmouth

Research Article | Vol. 12, No. 11 / 1 Nov 2021 / Biomedical Optics Express 6995
Biomedical Optics EXPRESS

Ultracompact fluorescence smartphone attachment using built-in optics for protoporphyrin-IX quantification in skin

BRADY HUNT,[1,*] SAMUEL S. STREETER,[1] ALBERTO J. RUIZ,[1] M. SHANE CHAPMAN,[2] AND BRIAN W. POGUE[1]

[1]Thayer School of Engineering, Dartmouth College, Hanover, New Hampshire 03755, USA
[2]Geisel School of Medicine, Department of Dermatology, Hanover, New Hampshire 03755, USA
[*]brady.hunt@dartmouth.edu

Abstract: Smartphone-based fluorescence imaging systems have the potential to provide convenient quantitative image guidance at the point of care. However, common approaches have required the addition of complex optical attachments, which reduce translation potential. In this study, a simple clip-on attachment appropriate for fluorescence imaging of protoporphyrin-IX (PpIX) in skin was designed using the built-in light source and ultrawide camera sensor of a smartphone. Software control for image acquisition and quantitative analysis was developed using the 10-bit video capability of the phone. Optical performance was characterized using PpIX in liquid tissue phantoms and endogenously produced PpIX in mice and human skin. The proposed system achieves a very compact form factor (<30 cm^3) and can be readily fabricated using widely available low-cost materials. The limit of detection of PpIX in optical phantoms was <10 nM, with good signal linearity from 10 to 1000 nM (R^2 >0.99). Both murine and human skin imaging verified that in vivo PpIX fluorescence was detected within 1 hour of applying aminolevulinic acid (ALA) gel. This ultracompact handheld system for quantification of PpIX in skin is well-suited for dermatology clinical workflows. Due to its simplicity and form factor, the proposed system can be readily adapted for use with other smartphone devices and fluorescence imaging applications. Hardware design and software for the system is made freely available on GitHub (https://github.com/optmed/CompactFluorescenceCam).

1. Introduction

Quantitative fluorescence measurement has become an essential tool in a wide range of biomedical applications and is increasingly utilized in medicine to provide image-guidance in diagnostic and therapeutic applications [1–4]. However, to achieve reliable quantitative performance, most fluorescence measurement systems require bulky and/or expensive instrumentation, including external light sources, filtering components, and highly sensitive detectors.

Recently, portable and handheld fluorescence imaging systems have been achieved by leveraging advances in mobile and embedded computing systems, including single board computers [5–8] and smartphones [9–18]. Smartphones, in particular, have become very sophisticated handheld optoelectronic systems that bring high-performance cameras, computing hardware, and touchscreen interfaces altogether in a very minimal form factor. The potential to leverage these built-in capabilities of modern smartphones has led to the development of smartphone-based imaging systems in an increasing range of in medical applications including: quantitative reading of point-of-care assays [19], microscopy [20], spectroscopy [21], and *in vivo* diagnostic imaging [22].

One promising application for smartphone-based *in vivo* fluorescence imaging is non-invasive, real-time assessment of epidermal and epithelial lesions [9–14]. In 2018, Song and Uthoff et al. reported one of the first smartphone-based *in vivo* fluorescence imaging systems, which

#439342 https://doi.org/10.1364/BOE.439342
Journal © 2021 Received 5 Aug 2021; revised 23 Sep 2021; accepted 24 Sep 2021; published 19 Oct 2021

Biomedical Optics EXPRESS

consisted of an Android smartphone, a case-like attachment with optical filters, a custom optical probe providing magnified image relay from the oral cavity, and external LED light source with battery supply [12,13]. The system was controlled by a custom Android application and corresponding web application for cloud-based image review and automated diagnostic classification. Autofluorescence and white light images from 170 patients undergoing diagnostic oral examination were acquired using the system and annotated by clinical experts. Smartphone-based fluorescence imaging in conjunction with an automated convolutional neural network classifier achieved 87% accuracy for prediction of normal versus suspicious for precancer. While impressive, two limitations of this smartphone-based implementation are that image quality was often suboptimal (>50% excluded after quality review) and the optical probe relied on careful alignment of external lenses with the smartphone camera, which could also impact image quality and translatability to other smartphone models.

In addition to autofluorescence tissue imaging, targeted fluorescence smartphone-based systems have been developed for sensing of protoporphyrin IX (PpIX), an endogenous fluorophore that is produced in mitochondria of cells as part of the heme synthesis pathway [23]. In the past two decades, system design for fluorescence quantification of PpIX has taken the form of point probe systems [24,25], imaging systems [26–28] and even diffuse tomographic systems [29,30]. The methods to separate the emission from the excitation light vary from spectrometer [31], to filter based cameras [26,32,33], to time-gated detection [34]. However, all of these implementations relied on bulky, scientific grade instrumentation. More recently, two smartphone-based implementations of PpIX sensing have been reported for monitoring of photodynamic therapy in dermal [9] and oral [10] tissues. Both systems include external LED light sources for blue (405nm) illumination as well as a >600 nm longpass filter mounted directly in front of the smartphone camera lens. While both systems represent a dramatic reduction in the cost/complexity of PpIX-sensing systems, both lacked onboard image analysis routines for real-time signal quantification and could potentially be further simplified by utilizing the native smartphone flash as a light source.

This study aimed to design an ultracompact fluorescence imaging attachment appropriate for imaging of PpIX in skin that overcomes the aforementioned limitations by leveraging the built-in LED flash as a light source in conjunction with an ultrawide camera sensor to achieve a very compact form factor. Specifically, the main goals of this work were to create and test:

- A fully passive attachment design that can be fabricated using widely available materials and achieves good quantitative fluorescence detection.
- Software to control the smartphone camera and perform real-time signal quantification using 10-bit video frames.
- Demonstration of real-time handheld operation of the system for *in vivo* detection of ALA-induced PpIX fluorescence in pre-clinical measurements of mice and human skin.

2. Methods

2.1. Optical system design

The ultracompact fluorescence attachment consisted of a clip-on attachment with embedded optical filtering components that mounts directly onto the phone's rear camera module (Fig. 1). The system includes a custom software application (app) that enables a video preview of the fluorescence signal and real-time intensity quantification. The clip attachment uses only passive optical elements and is designed for contact-based fluorescence measurement at the surface of the skin. This section details the design and fabrication of the hardware and software of our system.

Biomedical Optics EXPRESS

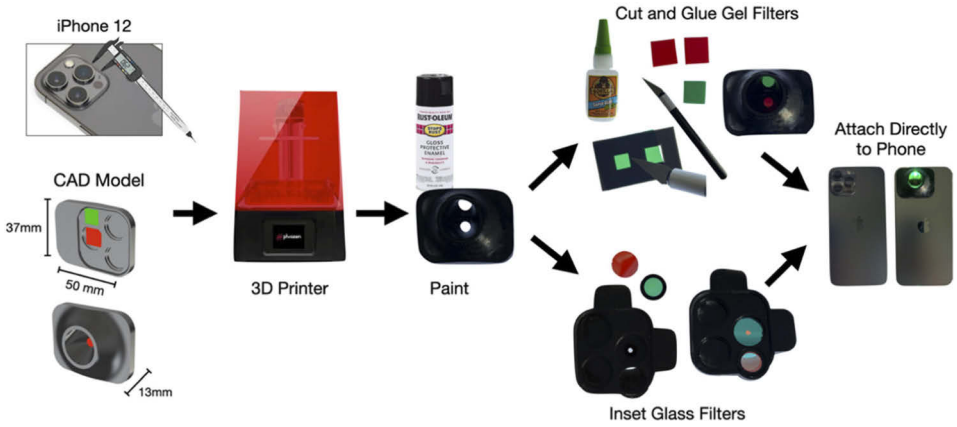

Fig. 1. Fabrication and assembly of ultracompact fluorescence attachment to the smartphone.

2.1.1. Phone and iOS application

The iPhone 12 Pro Max (Model MGCF3LL/A, Apple, Cupertino, USA) running iOS 14.5 was the platform used in this study. The phone's back camera module includes three separate sensors that operate at various magnifications. This study utilized the ultrawide camera module, which has a 1.54mm focal length and 120° collection angle. This camera was selected for two reasons: 1) proximity to the built-in flash and 2) relatively large field-of-view (FOV) at short working distances. The ultrawide camera utilizes a 1/3.6" CMOS sensor with 4032×3024 pixels (approximate individual pixel dimension of 1.0 micron/pixel). The camera module includes a dual-tone LED flash with 45 mW/cm^2 peak optical power, which was characterized using an optical power meter and spectrophotometer (see Section 2.2).

A custom iOS app called "Compact Fluorescence Camera" (abbreviated as CFCam) was developed in the Swift programming language using XCode 12.5 on a MacBook Pro running MacOS 11.4. When started, the app displays a live feed of the ultrawide camera feed and provides user interface controls to adjust the exposure, ISO, and intensity of the flash lighting. Visualization 1 provides a video demonstration of these user interface controls. The flash was configured to operate in a static 'torch' mode instead of dynamic 'flash' mode to provide constant illumination as the device is brought into contact with various points of interest on the skin. For real-time quantification of fluorescence signal, an average intensity calculation is performed using a 1280×720 pixel 10-bit video buffer. Minimum and maximum pixel intensities for the 10-bit video buffer were found to be 1,020 and 14,320 respectively. The average intensity from a 200×200 pixel square region of interest (ROI) is computed and displayed overlaid on the video feed in the user interface. When reporting the average intensity, the app first subtracts the minimum pixel value and rounds to the tens digit to mitigate frame-by-frame read noise. Mean ROI intensity as reported by the CFCam app was the quantitative metric utilized for PpIX signal quantification throughout this study. Source code for this iOS application is available on GitHub (https://github.com/optmed/CompactFluorescenceCam).

2.1.2. 3D printed attachment

The ultracompact fluorescence smartphone attachment design consists of a monolithic 3D printed enclosure with an internal recess to angle the built-in flash towards the camera sensor at a 1 cm working distance. Figure 1 provides a diagram of the fabrication and assembly process. The attachment design was created using SolidWorks 2020 (SolidWorks Corp., Waltham, MA, USA), and models were then converted into layer-by-layer printer files using CHITUBOX (v1.7.0) with

Biomedical Optics EXPRESS

the following printer settings: an individual layer height of 0.05 mm; six bottom layers, each with a 30-s exposure time; and a typical layer exposure time of 3 s. The models were printed using an LCD-based masked stereolithography 3D printer (Phrozen Sonic Mini) with a 50-micron axial resolution. The printer bulk material was eSUN black Standard Resin (Shenzhen eSUN Industrial Co., Shenzhen, China). The printing resolution provided sufficient tolerance to firmly attach the 3D printed component onto the back camera module without the need for adhesives. Because the 3D printing resin was slightly translucent after curing, the exterior of each printed component was painted black to improve the reflectivity of the inner light-guiding channels and ensure ambient lighting did not affect measurements. After painting, optical filters were inset into the attachment. Multiple versions of the attachment were fabricated to accommodate various optical filters as well as smaller/larger sampling FOV (Fig. 2). Detailed component lists with material costs (Dataset 1) Ref. [35] and 3D printing files (Dataset 2) for the five attachment designs (one using glass filters and four using lighting gel filters) evaluated in this study are made publicly available [36].

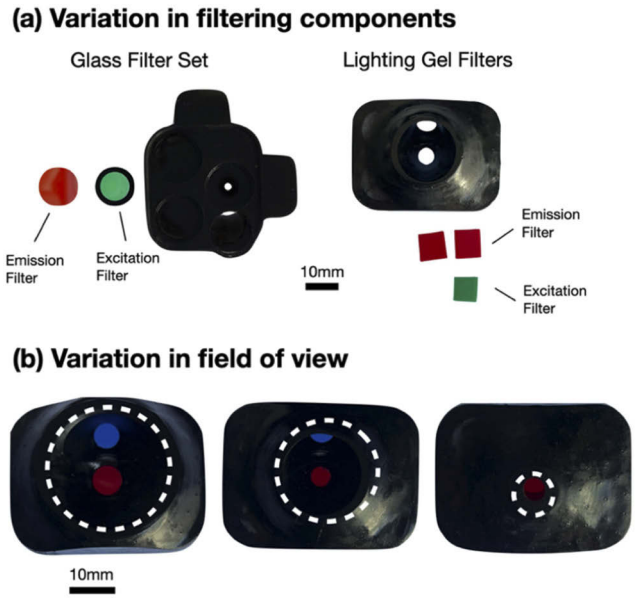

Fig. 2. Modularity in attachment design to accommodate various filter sets (a) and imaging fields of view (b).

2.2. Optical filter selection and characterization

The built-in LED camera flash contains two individual LEDs that are both illuminated when controlled using the CFCam app. Peak optical power was measured by bringing the bare LED in close contact with an optical power probe (PM200 with S120C probe, Thorlabs, New Jersey, USA). Additionally, the optical power throughput of each attachment was estimated by bringing the sample plane into contact with the power probe. The LED flash spectrum was measured using a probe-based spectrometer (Ocean Optics USB2000+, Ocean Optics Inc., Florida, USA) to determine which wavelengths could be utilized for PpIX excitation.

In order to use the built-in flash and nearby camera sensor, our filter selection constraints were threefold: 1) sufficiently small diameter (<13mm) and thickness (<5mm) to be placed directly in front of the smartphone flash and lens components, 2) high blocking efficiency of excitation light (OD ≥4), and 3) appropriate cut-on and cut-off wavelengths for PpIX excitation (400-550nm)

Biomedical Optics EXPRESS

and emission bands (600-700nm) given the LED emission spectra. A set of small diameter glass filters that met these criteria was identified and ordered directly from an optics vendor (stock #84-081 and #15-447, Edmund Optics, Barrington, New Jersey, USA). In addition to conventional glass filters, three lighting gel filters were also tested; these filters have a thickness of ~0.1mm and can readily be cut to any shape [37]. For filtering of the LED flash, two blue/green gel filter options were evaluated (stock #727 and #735, LEE Filters, Andover, England), and for longpass filtering of PpIX fluorescence a single red gel filter option was evaluated (LEE #106).

To characterize these filters, transmission spectra of each filter were acquired using the probe-based spectrometer and smartphone LED light source. All spectra were recorded with a 0.2 nm spectral resolution from 350 to 1000 nm. The spectrometer probe was mounted 1 cm away from the smartphone LED and the integration fixed to 20 µs to record the unfiltered LED spectrum. Individual filter spectra were then measured by directly inserting them in front of the smartphone LED. To estimate blocking efficiency, spectra were also acquired for each excitation and emission filter combination by stacking them inline and increasing the integration time to 200 ms. Filtered and unfiltered spectra were rescaled by their respective integration times and optical density (OD) calculated as follows:

$$OD_{\lambda} = -Log_{10}\tau_{\lambda}, \tag{1}$$

where τ_{λ} is the transmittance measured at each wavelength (λ). Blocking OD of the LED flash at the PpIX emission peak (OD_{634nm}) was compared for each filter set.

2.3. Fluorescence phantoms and sensitivity measurements

To assess the quantitative accuracy and sensitivity of the ultracompact fluorescence imaging system, a series of liquid fluorescence phantoms containing 1% intralipid and varying amounts of fluorophore (0.5 to 1000 nM PpIX) were measured. Phantom solutions were prepared using the methods described by Marois et al. [38] and are briefly summarized here. The negative control solution was 1% intralipid with no PpIX. A bulk quantity of the control solution was prepared by diluting Intralipid 20% w/v (NDC 0338-0519-09, Frensius Kabi/Baxter Healthcare) into 1x phosphate buffered saline to achieve 1% w/v. A small quantity of surfactant (Tween 20, P9416-50mL, Sigma-Aldrich Inc.) was then added at 0.1% v/v to improve the photostability of PpIX in solution. Next, powdered PpIX (P8293-1G, Sigma-Aldrich Inc.) was serially diluted 2:1 in dimethyl sulfoxide using 2 mL Eppendorf and a starting concentration of 100 µM. A fixed volume aliquot from each serial dilution was then pipetted into 25 cm^2 rectangular cell culture flasks (COR-430168, Corning) previously filled with approximately 50 mL of the 1% intralipid background solution. Each flask was then rocked to mix the PpIX, filled completely with the 1% intralipid solution to fill the container volume, and sealed with the flask cap. Transfer from Eppendorf tubes and dilution into the cell culture flasks constituted a fixed dilution factor of 100. Final PpIX concentrations of the liquid phantoms were 1000, 500, 250, 125, 62.5, 31.3, 15.6, 7.81, 3.91, 1.95, 0.977, 0.488, and 0 nM.

Measurements were acquired from each sample by taking a screen recording of the user interface real-time intensity calculation while placing the smartphone attachment directly in contact with the top surface of each flask. Contact was held for approximately 1-2 seconds to ensure the real-time intensity calculation stabilized, and each measurement was repeated in triplicate. The LED flash was set to full brightness, and the exposure time was fixed at 100 ms across all measurements. ISO speed was reduced when using glass filters to account for differences in transmission between glass and gel filters.

Linear regression of resulting measurements was performed in GraphPad Prism 9.1 (GraphPad Software, California, USA). Prior to linear fitting, data were rescaled to range from 0 to 1 using the minimum and maximum intensity readings obtained using each attachment and a log-log

Biomedical Optics EXPRESS

transformation was then applied. For visualization of the negative control sample on the log-log plot, a nominal value of below the lowest concentration was assigned (0.1 nM).

2.4. Pre-clinical in vivo murine measurements

All animal procedures were carried out following a protocol approved by the Committee for the Protection of Human Subjects, which is the Institutional Review Board (IRB) at Dartmouth College. Skin measurements of three nude mice were taken using the blue/red gel filter attachment with the smallest sampling FOV (5mm). The mice were athymic and fed a low-chlorophyll diet to mitigate tissue autofluorescence. A 10% ALA hydrochloride gel (Ameluz, Biofontera Inc., Massachusetts) was topically applied at two sites (the right leg and middle of the back) to induce PpIX accumulation in the skin, and the left leg was used as a control site. Measurements were taken at four time points: just prior to application (0 min) as well as 10, 60, and 180 min post-application. Mice remained anesthetized while applying the ALA gel and during pre- and post-application measurements (0 and 10 min), but were subsequently awakened and re-anesthetized for later measurements (60 and 180 min). Additionally, mice were kept in a dark environment in-between measurements to prevent photobleaching of the accumulated PpIX.

Camera acquisition settings remained fixed throughout all measurements with full LED brightness, 100 ms exposure, and 2300 ISO speed. For each measurement, the smartphone attachment was brought directly into contact with the skin and held for 1-2 s to allow the real-time intensity calculation to stabilize. Measurements were repeated three times at each site and at each time point. The maximum intensity reading across repeated measurements at each time was recorded and used to analyze fluorescence accumulation over time. Differences in mean intensity between the right and left legs at each time point were compared using a paired t-test (with $p<0.05$ considered statistically significant). Widefield fluorescence images were also acquired at each time point using a previously developed smartphone-based PpIX dosimeter to qualitatively verify the location and intensity of fluorescence accumulation [9].

2.5. Pre-clinical in vivo human measurements

Human skin measurements were performed on four healthy adult volunteers who gave informed consent to participate in the study following a protocol approved by the Dartmouth College Institutional Review Board. Measurements were taken on the underside of the forearm with the palm facing up. A site for ALA gel application was demarcated using a rectangular piece of black tape with a 10 mm diameter circular region cut out. The tissue regions on the forearm just outside the tape were used as control sites and were also sampled at each time point. A 10% ALA gel (Ameluz, Biofontera Inc., Massachusetts) was applied to the inside the taped region of the forearm and allowed to dry in open air for 10 min, after which the first measurement was taken. Subsequent measurements were taken at 60, 180, and 240 min time points, with the site remaining covered from light exposure between measurements using a layer of plastic wrap and an additional layer of black tape.

The 5mm FOV attachment (same as the murine measurements) was utilized with fixed acquisition settings of 100 ms and 2300 ISO speed. Measurements were taken in ambient room lighting and by repeatedly bringing the device in contact with the skin and holding for 2-3 s. This was done three times at tissue sites outside the taped region and three times inside the taped region, with the maximum intensity reading recorded and used for analysis. Differences in mean intensity between the taped application region and control sites at each time point were compared using a paired t-test. Widefield fluorescence images were also acquired at each time point using a previously developed smartphone-based PpIX dosimeter [9].

Biomedical Optics EXPRESS

3. Results

Figure 3 shows the transmission spectra for the smartphone LED flash overlaid on the absorption and fluorescence spectra of PpIX. The LED light source spans most of the visible spectrum (430 to 750 nm), although notably the LED spectra does not extend to the 405 nm Soret band peak excitation wavelength for PpIX. Therefore, the excitation cut-on and cut-off wavelengths were determined to be approximately 440 to 560 nm, with a ≥600 nm longpass as the emission filter. The optical power of the unfiltered LED was 45 mW/cm^2 when the flash was in direct contact with the power meter and 7 mW/cm^2 passing through the angled flash channel to a 18 mm diameter circular sample plane.

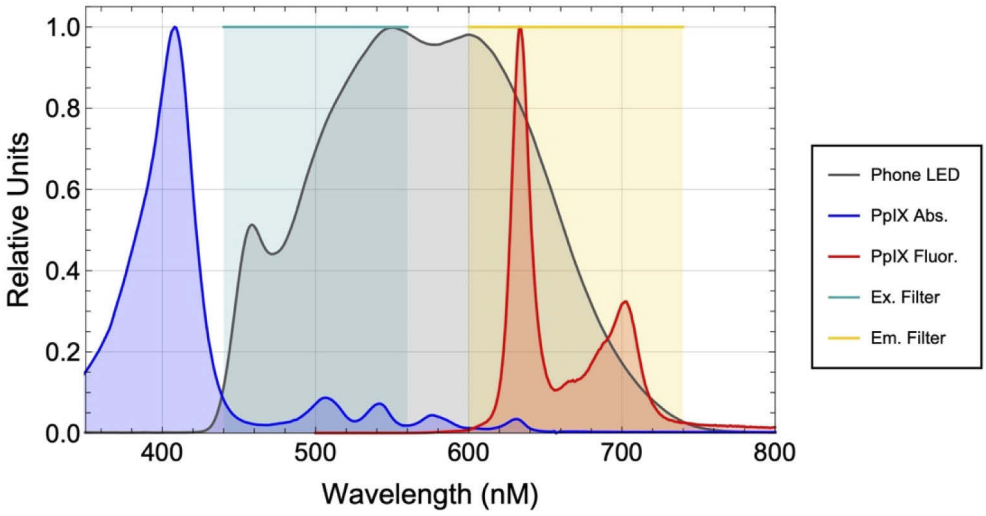

Fig. 3. Transmission spectra of smartphone flash LED overlaid on absorption and fluorescence spectra of PpIX. Proposed excitation and emission filter ranges to utilize the phone LED and camera sensor are highlighted.

Figure 4 contains spectra for three optical filter sets with adequate blocking OD for PpIX detection. All three filter options achieved separabililty of excitation and emission wavelengths with OD≥4 in the PpIX fluorescence window. Peak transmission was substantially higher for glass filtering components than for gel filters (99% vs 40%), although when used in tandem the glass filter set had a lower blocking OD for rejection of the flash LED and therefore a higher noise floor (OD 4.6 vs 5.5 for glass and gel filters, respectively). Several other excitation gel filter options with higher transmission were also evaluated, but none of them achieved sufficient blocking OD to ensure adequate rejection of background signal to detect faint PpIX fluorescence signals (data not shown).

Figure 5 demonstrates the CFCam app user interface controls and real-time signal quantification functionality. When launched, the app is initialized with a live preview of the ultrawide camera feed with a 200 × 200 pixel ROI overlaid to indicate the region from which average intensity is calculated (Fig. 5(a)). A lock icon toggles the acquisition setting controls for camera sensor, exposure, ISO speed, and LED brightness. Figure 5(b) provides screenshots of real-time intensity calculation for attachments with 30 mm, 18 mm, and 5 mm diameter sampling FOV.

Figure 6 provides linear regression results from serial dilution of PpIX in 1% intralipid phantoms across five different attachment versions. Optical power delivered to the sampling plane varied based on the filter selection and ranged between 0.1 to 2.0 mW/cm^2, with the lowest/highest throughputs being the small FOV gel filter and glass filter attachments, respectively; however, the material cost of the glass filters attachment was $ 250 USD compared to under $1 for gel filters

Biomedical Optics EXPRESS

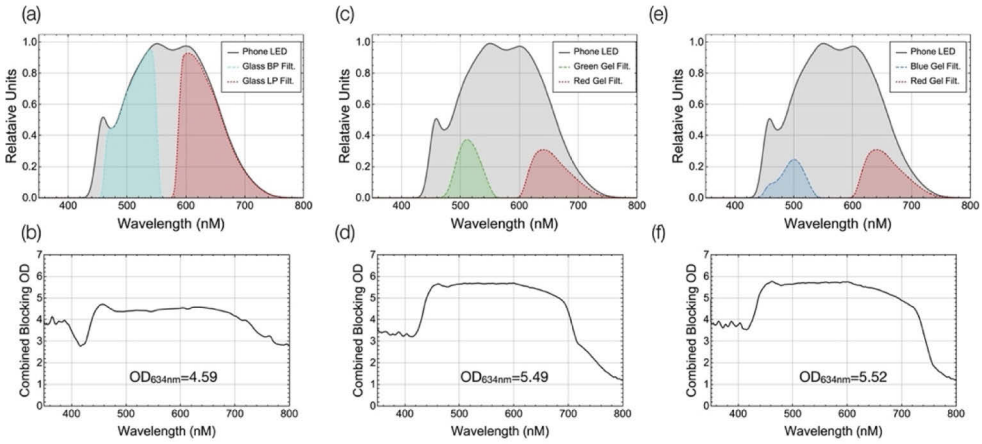

Fig. 4. Transmission spectra and blocking efficiency of three filter sets evaluated with the proposed fluorescence attachment: (a-b) glass filters, (c-d) red/green gel filters, (e-f) blue/green gel filters.

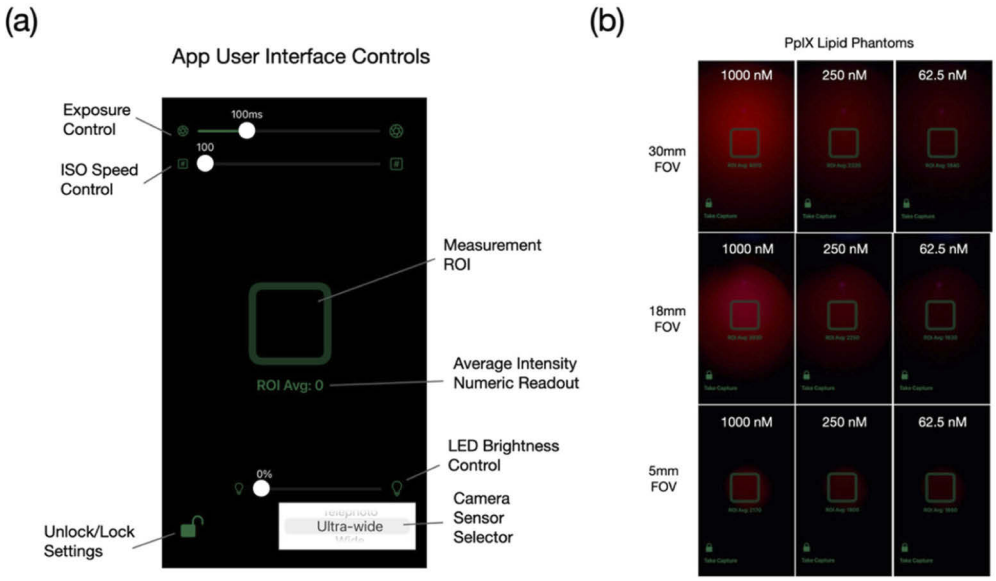

Fig. 5. CFCam smartphone app user interface for control of acquisition parameters and real-time fluorescence intensity quantification. (a) Labeled screenshot of app user interface. (b) Screenshots of real-time intensity calculation for attachments with 30 mm, 18 mm, and 5 mm sample plane field-of-view diameter.

(Dataset 1, Ref. [35]). Despite these differences in optical efficiency, signal linearity from 10 to 1000 nM was excellent (R^2>0.99) for both glass filter and gel filter attachments.

Figure 7 contains results from *in vivo* pre-clinical measurements of ALA-induced PpIX fluorescence in animal and human skin. No fluorescence accumulation was observed at the 10 min post-application of the ALA gel. At 60 min post-ALA gel application, however, a statistically significant increase in normalized fluorescence intensity was observed in both murine and human subjects (control vs ALA gel, mice: 3.75 vs 1.04, $p<0.05$; human: 1.33 vs 1.09, $p<0.05$). The PpIX fluorescence accumulation further increased at the 180 min time point, with some systemic

Biomedical Optics EXPRESS

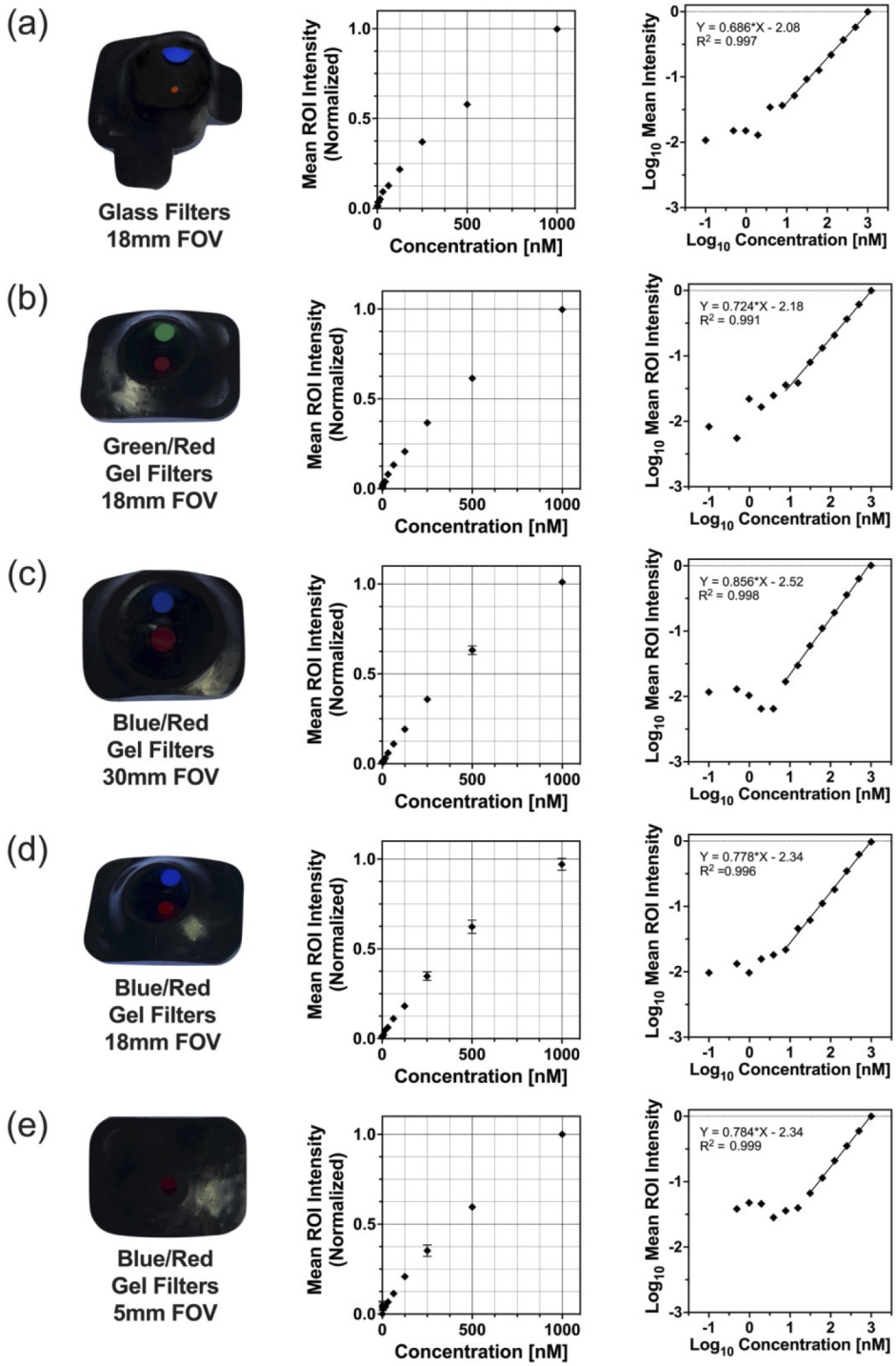

Fig. 6. Signal linearity from serial dilution of PpIX in 1% intralipid solution using five different attachment versions with varying filtering components and sampling field-of-view. Left: image of assembled attachment. Middle: linear scatter plot of normalized intensity measurements. Error bars indicate ± one standard deviation from the mean based on three repeat measurements. Right: Log-log plot of measured intensities averaged across all replicates with linear regression fit overlaid.

Biomedical Optics EXPRESS

PpIX production detected at the control site in the murine measurements (control vs ALA gel, mice: 11.6 vs 5.21, $p<0.01$; human: 2.01 vs 1.10, $p<0.05$). Visualization 2 provides a video demonstration of an *in vivo* measurement being taken at both control and ALA gel sites on the forearm of a healthy adult volunteer.

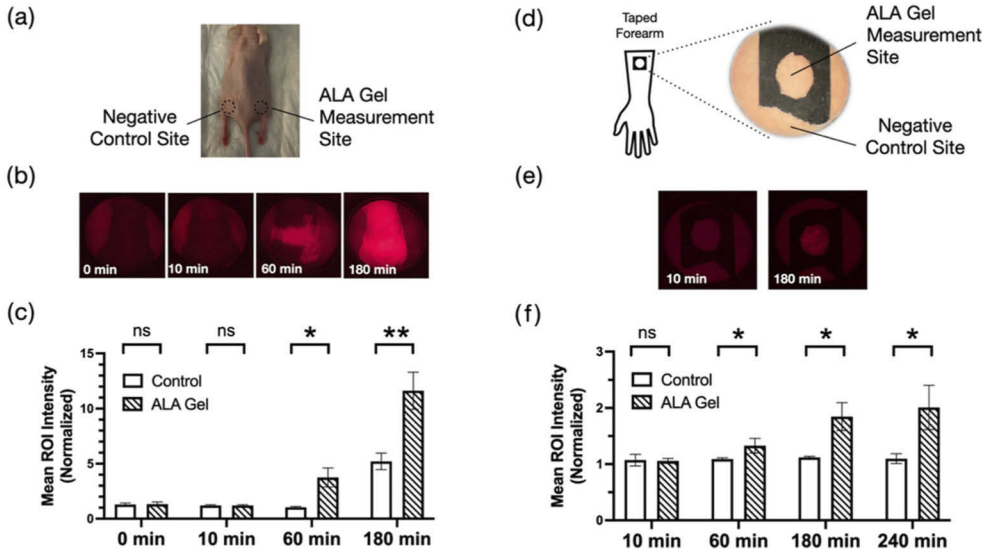

Fig. 7. *In vivo* measurement of PpIX fluorescence using smartphone system in mice and human skin after application of aminolevulinic (ALA) gel. (a and d) Annotated white light images of experimental setup. In mice, ALA gel was applied to the right leg and mid-back of the mouse and the left leg was used as a control imaging site. In humans, black tape with a circular cutout was used to demarcate the application site on the forearm. (b and e) Widefield fluorescence images acquired with a secondary imaging system [9] to confirm PpIX fluorescence accumulation over time. (c and f) Mean intensity of control and ALA sites measured at each time point using the proposed ultracompact smartphone system. Error bars indicate ± one standard deviation from the mean based on three repeat measurements. Statistical significance testing was performed using a paired t-test at each time point. The following symbols indicate p-value results as follows: ns ($P>0.05$), *($P\leq0.05$), **($P\leq0.01$).

4. Discussion

In recent years, there has been robust growth in the development of smartphone-based imaging systems for biomedical imaging applications [21,22]. However, the degree to which the native optics are leveraged varies greatly from application to application, and the addition of more complex active optics to the phone simply reduces the potential for wider adoption. In this study, an ultracompact attachment design was developed, which leverages the on-board optics for quantitative measurement of PpIX fluorescence in skin. The key features used were (1) exploitation of green wavelengths for PpIX excitation fitting with the available spectrum of the flash, and (2) use of the ultrawide camera lens, which provided good signal quantification at a short working distance.

The compactness and capability for real-time signal quantification of the system give it high potential to be utilized in dermatological settings for monitoring and personalization of PDT treatment regimens or measurement of PpIX in other clinical settings such as wound assessment [39,40], lesion identification [41,42], porphyria [43,44]. In intralipid phantoms, the system achieved excellent linearity down to 10 nM, and was able to detect PpIX fluorescence

Biomedical Optics EXPRESS

accumulation in both murine and human skin. This sensitivity is similar to a previously developed system by Ruiz et al. [9] which utilized a 405nm LED ring for Soret peak excitation, but also had a larger working distance of 72mm. We hypothesize that the limit of detection of this short working distance attachment could be further improved if an external 405nm LED was utilized in place of filtering the built-in flash LED, but with the trade-off of significantly increasing the cost/complexity of the design. The proposed attachment was <30 cm^3 in volume and had an insignificant material cost of less than $1 USD when implemented with lighting gel filters.

While the attachment models in this study were specific to the Apple iPhone 12, the model design can be readily adapted to any smartphone model by adjusting the attachment layout using computer aided design software. The proposed attachment was designed for contact-based sampling of the skin. This approach is helpful for fluorescence measurement in two important ways: 1) shielding the measurement from external room lighting and 2) ensuring consistent sampling with regards to field of view and distance. A variety of attachment designs with sampling field of view ranging from 5 to 30 mm were demonstrated in this study. In dermatological applications, these relatively small fields of view can facilitate easier sampling of moderately curved tissues (for example, near the cheek bones and eyes). Additionally, this sampling field of view can readily be modified in the 3D printed design to suit various applications. The system's hardware and software design are both publicly available and can be adapted for other contact-based fluorescence intensity measurement applications. This open-source, modular design provides proof of principle for integrating optical filters with the cameras and light sources native to smartphones in order to achieve sensitive fluorescence quantification.

There are limitations of the present study as well as areas for further improvement of this ultracompact design. Although the proposed system should be feasible for any smartphone system with an LED flash and camera, the current software for real-time analysis is only compatible with iOS devices. Additionally, the 10-bit video frame analysis routine only provides relative intensity information and would need to be calibrated for each camera sensor in order to provide absolute quantification across multiple phone models. The pre-clinical measurements were only performed on small sample sizes as a proof of principle for demonstrating its capability for *in vivo* measurements. For human clinical use, there may be additional factors which could impact background fluorescence signatures (diet, metabolism, and skin pigmentation, for example). Although the amount of topical gel applied to both murine and human tissues was similar, an increase in PpIX fluorescence was observed at 180 min, whereas no increase in control fluorescence was observed in humans (Fig. 7(c) and 7(f)). We hypothesize that this differential increase in background fluorescence was a result of systemic ALA uptake and PpIX production due to the thin dermal tissue layer and much higher metabolic rate of the mice. Further work is needed characterize the impact of these factors in order to establish robust intrasubject PpIX fluorescence quantification. Further work to translate this system into clinical trials and evaluate the utility in the hands of non-technical team members is ongoing.

In conclusion, a simple passive attachment was prototyped and tested for use with a smartphone, to allow quantification of PpIX with the native opto-electronics on the device. The use of gel filters and 3D printed clip-on design result in an ultracompact, handheld fluorescence sensing platform, with green wavelength band excitation and red wavelength emission. The detection threshold was sufficient to detect biologically relevant PpIX levels in both mice and human skin, and the temporal kinetics of production were followed. The device design and software prototype are available as an open-source project on GitHub, to allow further testing and use of this translatable approach by other laboratories.

Funding. National Cancer Institute (P01 CA084203).

Acknowledgments. The authors would like to thank Arthur Petusseau for assisting with the murine measurements and Dr. Petr Bruza for helpful discussions and input on the optical attachment design.

Disclosures. The authors report no conflicts of interest.

Biomedical Optics EXPRESS

Data availability. A list of components (Dataset 1) Ref. [35] and 3D design files (Dataset 2) are made available with this publication [36]. Software related to this research is publicly available on GitHub [45]. Data underlying the results presented in this paper are not publicly available at this time but may be obtained from the authors upon reasonable request.

References

1. F. Leblond, S. C. Davis, P. A. Valdés, and B. W. Pogue, "Pre-clinical whole-body fluorescence imaging: review of instruments, methods and applications," J. Photochem. Photobiol., B **98**(1), 77–94 (2010).
2. D. Grosenick, H. Rinneberg, R. Cubeddu, and P. Taroni, "Review of optical breast imaging and spectroscopy," J. Biomed. Opt. **21**(9), 091311 (2016).
3. L. Sauer, K. M. Andersen, C. Dysli, M. S. Zinkernagel, P. S. Bernstein, and M. Hammer, "Review of clinical approaches in fluorescence lifetime imaging ophthalmoscopy," J. Biomed. Opt. **23**(09), 1–20 (2018).
4. S. Hernot, L. van Manen, P. Debie, J. S. D. Mieog, and A. L. Vahrmeijer, "Latest developments in molecular tracers for fluorescence image-guided cancer surgery," Lancet Oncol. **20**(7), e354–e367 (2019).
5. C. Li, P. Liu, P. Shao, J. Pei, Y. Li, T. M. Pawlik, E. W. Martin, and R. X. Xu, "Handheld projective imaging device for near-infrared fluorescence imaging and intraoperative guidance of sentinel lymph node resection," J. Biomed. Opt. **24**(08), 1 (2019).
6. S. Parra, E. Carranza, J. Coole, B. Hunt, C. Smith, P. Keahey, M. Maza, K. Schmeler, and R. Richards-Kortum, "Development of low-cost point-of-care technologies for cervical cancer prevention based on a single-board computer," IEEE J. Transl. Eng. Health Med. **8**, 1–10 (2020).
7. U. Obahiagbon, J. T. Smith, M. Zhu, B. A. Katchman, H. Arafa, K. S. Anderson, and J. M. Blain Christen, "A compact, low-cost, quantitative and multiplexed fluorescence detection platform for point-of-care applications," Biosens. Bioelectron. **117**, 153–160 (2018).
8. A. Huttunen, S. Aikio, M. Kurkinen, J.-T. Makinen, R. Mitikka, L. Kivimaki, M. Harjumaa, J. Takalo-Mattila, C. Liedert, J. Hiltunen, and L. Hakalahti, "Portable low-cost fluorescence reader for LFA measurements," IEEE Sensors J. **20**(17), 10275–10282 (2020).
9. A. J. Ruiz, E. P. M. Larochelle, J. R. Gunn, S. M. Hull, T. Hasan, M. S. Chapman, and B. W. Pogue, "Smartphone fluorescence imager for quantitative dosimetry of protoporphyrin-IX-based photodynamic therapy in skin," J. Biomed. Opt. **25**(6), 1–13 (2019).
10. S. Khan, M. A. B. Hussain, A. P. Khan, H. Liu, S. Siddiqui, S. Mallidi, P. Leon, L. Daly, G. Rudd, F. Cuckov, C. Hopper, S. G. Bown, K. Akhtar, S. A. Hasan, S. A. Siddiqui, T. Hasan, and J. P. Celli, "Clinical evaluation of smartphone-based fluorescence imaging for guidance and monitoring of ALA-PDT treatment of early oral cancer," J. Biomed. Opt. **25**(06), 1–10 (2020).
11. R. Uthoff, B. Song, M. Maarouf, V. Shi, and R. Liang, "Point-of-care, multispectral, smartphone-based dermascopes for dermal lesion screening and erythema monitoring," J. Biomed. Opt. **25**(06), 1–21 (2020).
12. B. Song, S. Sunny, R. D. Uthoff, S. Patrick, A. Suresh, T. Kolur, G. Keerthi, A. Anbarani, P. Wilder-Smith, M. A. Kuriakose, P. Birur, J. J. Rodriguez, and R. Liang, "Automatic classification of dual-modalilty, smartphone-based oral dysplasia and malignancy images using deep learning," Biomed. Opt. Express **9**(11), 5318–5329 (2018).
13. R. D. Uthoff, B. Song, S. Sunny, S. Patrick, A. Suresh, T. Kolur, G. Keerthi, O. Spires, A. Anbarani, P. Wilder-Smith, M. A. Kuriakose, P. Birur, and R. Liang, "Point-of-care, smartphone-based, dual-modality, dual-view, oral cancer screening device with neural network classification for low-resource communities," PLoS One **13**(12), e0207493 (2018).
14. B. D. Grant, T. Quang, J. C. Possati-Resende, C. Scapulatempo-Neto, G. de Macedo Matsushita, E. C. Mauad, M. H. Stoler, P. E. Castle, J. H. T. Guerreiro Fregnani, K. M. Schmeler, and R. Richards-Kortum, "A mobile-phone based high-resolution microendoscope to image cervical precancer," PLoS One **14**(2), e0211045 (2019).
15. C. Vietz, M. L. Schütte, Q. Wei, L. Richter, B. Lalkens, A. Ozcan, P. Tinnefeld, and G. P. Acuna, "Benchmarking smartphone fluorescence-based microscopy with DNA origami nanobeads: reducing the gap toward single-molecule sensitivity," ACS Omega **4**(1), 637–642 (2019).
16. V. Müller, J. M. Sousa, H. Ceylan Koydemir, M. Veli, D. Tseng, L. Cerqueira, A. Ozcan, N. F. Azevedo, and F. Westerlund, "Identification of pathogenic bacteria in complex samples using a smartphone based fluorescence microscope," RSC Adv. **8**(64), 36493–36502 (2018).
17. Y. Liu, A. M. Rollins, R. M. Levenson, F. Fereidouni, and M. W. Jenkins, "Pocket MUSE: an affordable, versatile and high-performance fluorescence microscope using a smartphone," Commun. Biol. **4**(1), 334 (2021).
18. Q. Deng, Z. Lan, L. Xu, Z. Zhu, and X. Shu, "A miniaturized apparatus based on a smartphone for microsecond-resolved luminescence lifetime imaging," Sens. Actuators, B **343**, 130086 (2021).
19. S. Kanchi, M. I. Sabela, P. S. Mdluli, Inamuddin, and K. Bisetty, "Smartphone based bioanalytical and diagnosis applications: a review," Biosens. Bioelectron. **102**, 136–149 (2018).
20. W. Zhu, C. Gong, N. Kulkarni, C. D. Nguyen, and D. Kang, "Smartphone-based microscopes," in *Smartphone Based Medical Diagnostics* (Elsevier, 2020), pp. 159–175.
21. I. Hussain and A. K. Bowden, "Smartphone-based optical spectroscopic platforms for biomedical applications: a review [Invited]," Biomed. Opt. Express **12**(4), 1974 (2021).
22. B. Hunt, A. J. Ruiz, and B. W. Pogue, "Smartphone-based imaging systems for medical applications: a critical review," J. Biomed. Opt. **26**(04), 040902 (2021).

Biomedical Optics EXPRESS

23. J. Leveckis, J. L. Burn, N. J. Brown, and M. W. Reed, "Kinetics of endogenous protoporphyrin IX induction by aminolevulinic acid: preliminary studies in the bladder," J. Urol. **152**(2 Part 1), 550–553 (1994).
24. D. W. Roberts, P. A. Valdés, B. T. Harris, K. M. Fontaine, A. Hartov, X. Fan, S. Ji, S. S. Lollis, B. W. Pogue, F. Leblond, T. D. Tosteson, B. C. Wilson, and K. D. Paulsen, "Coregistered fluorescence-enhanced tumor resection of malignant glioma: relationships between δ-aminolevulinic acid-induced protoporphyrin IX fluorescence, magnetic resonance imaging enhancement, and neuropathological parameters. Clinical article," J. Neurosurg. **114**(3), 595–603 (2011).
25. B. W. Pogue, C. Sheng, J. Benevides, D. Forcione, B. Puricelli, N. Nishioka, and T. Hasan, "Protoporphyrin IX fluorescence photobleaching increases with the use of fractionated irradiation in the esophagus," J. Biomed. Opt. **13**(3), 034009 (2008).
26. H. Heyerdahl, I. Wang, D. L. Liu, R. Berg, S. Andersson-Engels, Q. Peng, J. Moan, S. Svanberg, and K. Svanberg, "Pharmacokinetic studies on 5-aminolevulinic acid-induced protoporphyrin IX accumulation in tumours and normal tissues," Cancer Lett. **112**(2), 225–231 (1997).
27. F. Fischer, E. F. Dickson, J. C. Kennedy, and R. H. Pottier, "An affordable, portable fluorescence imaging device for skin lesion detection using a dual wavelength approach for image contrast enhancement and aminolaevulinic acid-induced protoporphyrin IX. Part II. In vivo testing," Lasers Med. Sci. **16**(3), 207–212 (2001).
28. A. Bogaards, A. Varma, S. P. Collens, A. Lin, A. Giles, V. X. D. Yang, J. M. Bilbao, L. D. Lilge, P. J. Muller, and B. C. Wilson, "Increased brain tumor resection using fluorescence image guidance in a preclinical model," Lasers Surg. Med. **35**(3), 181–190 (2004).
29. J. D. Gruber, A. Paliwal, V. Krishnaswamy, H. Ghadyani, M. Jermyn, J. A. O'Hara, S. C. Davis, J. S. Kerley-Hamilton, N. W. Shworak, E. V. Maytin, T. Hasan, and B. W. Pogue, "System development for high frequency ultrasound-guided fluorescence quantification of skin layers," J. Biomed. Opt. **15**(2), 026028 (2010).
30. D. S. Kepshire, S. L. Gibbs-Strauss, S. L. Gibbs-Struass, J. A. O'Hara, M. Hutchins, N. Mincu, F. Leblond, M. Khayat, H. Dehghani, S. Srinivasan, and B. W. Pogue, "Imaging of glioma tumor with endogenous fluorescence tomography," J. Biomed. Opt. **14**(3), 030501 (2009).
31. R. H. Pottier, Y. F. Chow, J. P. LaPlante, T. G. Truscott, J. C. Kennedy, and L. A. Beiner, "Non-invasive technique for obtaining fluorescence excitation and emission spectra in vivo," Photochem. Photobiol. **44**(5), 679–687 (1986).
32. C. S. Betz, H. Stepp, P. Janda, S. Arbogast, G. Grevers, R. Baumgartner, and A. Leunig, "A comparative study of normal inspection, autofluorescence and 5-ALA-induced PPIX fluorescence for oral cancer diagnosis," Int. J. Cancer **97**(2), 245–252 (2002).
33. W. Stummer, H. Stepp, G. Möller, A. Ehrhardt, M. Leonhard, and H. J. Reulen, "Technical principles for protoporphyrin-IX-fluorescence guided microsurgical resection of malignant glioma tissue," Acta Neurochir. **140**(10), 995–1000 (1998).
34. M-A. E. J. Ortner, B. Ebert, E. Hein, K. Zumbusch, D. Nolte, U. Sukowski, J. Weber-Eibel, B. Fleige, M. Dietel, M. Stolte, G. Oberhuber, R. Porschen, B. Klump, H. Hörtnagl, H. Lochs, and H. Rinneberg, "Time gated fluorescence spectroscopy in Barrett's oesophagus," Gut **52**(1), 28–33 (2003).
35. B. Hunt, "Part specifications and material cost for a smartphone-based fluorescence imaging system," figshare (2021), https://doi.org/10.6084/m9.figshare.15105027.
36. B. Hunt, "3D models of optical attachments for smartphone-based fluorescence quantification," figshare (2021), https://doi.org/10.6084/m9.figshare.15105006.
37. A. J. Ruiz, M. K. Giallorenzi, B. Hunt, K. S. Samkoe, and B. W. Pogue, "Lighting gel filters as low-cost alternatives for fluorescence imaging and optical system design," (Under Review).
38. M. Marois, J. Bravo, S. C. Davis, and S. C. Kanick, "Characterization and standardization of tissue-simulating protoporphyrin IX optical phantoms," J. Biomed. Opt. **21**(3), 035003 (2016).
39. M. C. S. Vallejo, N. M. M. Moura, A. T. P. C. Gomes, A. S. M. Joaquinito, M. A. F. Faustino, A. Almeida, I. Gonçalves, V. V. Serra, and M. G. P. M. S. Neves, "The role of porphyrinoid photosensitizers for skin wound healing," Int. J. Mol. Sci. **22**(8), 4121 (2021).
40. L. Le, M. Baer, P. Briggs, N. Bullock, W. Cole, D. DiMarco, R. Hamil, K. Harrell, M. Kasper, W. Li, K. Patel, M. Sabo, K. Thibodeaux, and T. E. Serena, "Diagnostic accuracy of point-of-care fluorescence imaging for the detection of bacterial burden in wounds: results from the 350-patient fluorescence imaging assessment and guidance trial," Advances in Wound Care **10**(3), 123–136 (2021).
41. H. Yu, T. S. Ho, H. Kang, Y. Bae, E. H. Choi, S. H. Choi, and B. Jung, "Use of digital photography to identify neoplastic skin lesions after labelling by ALA-derived protoporphyrin," J. Porphyrins Phthalocyanines **25**(04), 307–313 (2021).
42. D. Ihara, H. Hazama, T. Nishimura, Y. Morita, and K. Awazu, "Fluorescence detection of deep intramucosal cancer excited by green light for photodynamic diagnosis using protoporphyrin IX induced by 5-aminolevulinic acid: an ex vivo study," J. Biomed. Opt. **25**(06), 1 (2020).
43. A. K. Dickey, C. Quick, S. Ducamp, Z. Zhu, Y.-C. A. Feng, H. Naik, M. Balwani, K. E. Anderson, X. Lin, J. E. Phillips, L. Rebeiz, H. L. Bonkovsky, B. M. McGuire, B. Wang, D. I. Chasman, J. W. Smoller, M. D. Fleming, and D. C. Christiani, "Evidence in the UK Biobank for the underdiagnosis of erythropoietic protoporphyria," Genet. Med. **23**(1), 140–148 (2021).
44. M. Sachar, K. E. Anderson, and X. Ma, "Protoporphyrin IX: the good, the bad, and the ugly," J. Pharmacol. Exp. Ther. **356**(2), 267–275 (2016).

Biomedical Optics EXPRESS

45. B. Hunt, "CFCam: software and design files for an ultracompact fluorescence smartphone attachment," Github (2021), https://github.com/optmed/CompactFluorescenceCam.